

Enhanced absorption of weak ultrashort light pulses by a narrowband atomic mediumA. J. A. Carvalho ¹, R. S. N. Moreira ¹, J. Ferraz ², S. S. Vianna ¹, L. H. Acioli ¹, and D. Felinto ^{1,*}¹*Departamento de Física, Universidade Federal de Pernambuco, 50670-901 Recife, Pernambuco, Brazil*²*Departamento de Física, Universidade Federal Rural de Pernambuco, 52171-900 Recife, Pernambuco, Brazil*

(Received 21 November 2019; accepted 26 March 2020; published 15 May 2020; corrected 28 May 2020)

The storage of broadband single photons from a parametric-down-conversion source is a capability with the potential to foster significant development in the field of quantum information. A particular challenge to this problem, however, is the mismatch between the short-lived photon and the long-lived memories, which translates into quite different frequency bands for the two systems. Ultimately, this difficulty can be mapped into the problem of how a narrowband medium can efficiently absorb a broadband pulse of light. Here we present a detailed approach to this problem focusing on the absorption of photons at 800 nm, a common choice for parametric-down-conversion sources, by hot vapors of rubidium atoms. For this, we employ a stronger control field to drive a sequential two-photon transition on the atoms, which is intrinsically broadband, together with a weak signal field consisting of a femtosecond pulse of light. We describe then how to measure small absorptions of the signal pulse and how to improve this absorption through the various parameters of the problem. Our results are modeled by a perturbative theory suitable to our present weak-absorption regime. Finally, we provide a road map with different strategies to achieve larger absorptions.

DOI: [10.1103/PhysRevA.101.053426](https://doi.org/10.1103/PhysRevA.101.053426)**I. INTRODUCTION**

The generation of photon pairs from spontaneous parametric down conversion (SPDC) is a cornerstone technique in the field of quantum optics [1], directly responsible for great progress in fundamental physics and diverse applications [2], particularly in the field of quantum information [3]. The probabilistic nature of SPDC, however, prevents its application to more complex problems that demand scalability, since the probability to generate many photon pairs simultaneously decreases exponentially with the number of pairs. A possible way to circumvent this problem is to store the photon in a memory for later use, relaxing then the requirement of simultaneous generation. Significant advances have been made in recent years in the development of quantum memories for various applications [4,5]. However, the ultra-broadband nature of the SPDC photon, with bandwidths in excess of 10 THz, introduces a number of extra difficulties in the development of a compatible memory. At the heart of the problem is the fact that memories typically have small bandwidths, associated with their long coherence times, and the ultrafast SPDC photons maximize all issues arising from this mismatch. On the other hand, in 2016, Costanzo *et al.* demonstrated the coherent propagation of ultrashort single-photon pulses through an atomic medium, by measuring its strong deformation by the narrowband atomic medium [6]. At the time, it was suggested this observation could pave the way to new quantum memories for ultrashort single photons. Here we detail this proposal and report the first steps, both theoretically and experimentally, for its implementation.

The process of storing information of a short pulse of light into a long-lived memory, with bandwidth much smaller than

that of the flying photons, is the starting point of any quantum memory for light. The most common approach to this task is to use a two-photon Λ transition between two ground states, which is intrinsically broadband, with all spectral components of the light pulse participating in the process. This configuration may involve a resonant excited state, through the effects of electromagnetically induced transparency [7,8] and Autler-Townes splitting [9], or pure Raman transitions [10,11]. When using ensembles of alkali atoms for storage, this approach will be typically limited in bandwidth to a few GHz, determined by the splitting between the two ground states. In order to use memories of this kind with the SPDC photons, the most common approach is to substantially decrease the photonic bandwidth by placing the parametric-down-conversion source inside a narrowband optical cavity [12–15]. The bandwidth narrowing of photons from SPDC to the GHz range, by band-pass filters, is also employed in solid-state memories based on excited states with a combination of large inhomogeneous broadening and narrow homogeneous bandwidth [16,17].

There are, however, interesting aspects to explore in memories that could bridge directly from an ultrashort photon to a long-lived atomic state. First, it opens the possibility to explore the femtosecond pulse duration to enhance the speed of various tasks. Second, such pulse durations are usually much shorter than any decoherence time of atomic systems, leading to the possibility of incorporating coherent control techniques to write and manipulate the stored information [18]. The first experimental approach to store femtosecond photons in long-lived memories explore Raman transitions in atomic or solid-state systems with large ground-state separations, on the THz range. So far, implementations along this line have been reported in molecular hydrogen [19,20], diamond [21], and barium atoms [22].

Here we propose a different pathway for the storage of ultrashort photons in atomic ensembles, employing two-photon

*Corresponding author: dfelinto@df.ufpe.br

cascade transitions to long-lived excited states. This approach is considerably less restricted in terms of atomic species for the memory than the present alternatives relying on Raman transitions between ground states with THz frequency separations. There are many more options of suitable state separations among excited states of basically any atom. To illustrate this fact, we conduct our study with one of the most common atomic systems for various applications, a hot ensemble of rubidium atoms, excited by light around 800 nm, also a common choice coming from femtosecond Ti:sapphire lasers. Even though the final excited state of our choice, $5D_{3/2}$, has a lifetime of only 240 ns, this is already 10^6 times the excitation-pulse durations, around 100 fs. Longer lifetimes, when required, could be achieved through a second excitation stage by longer pulses, which would transfer the atoms at $5D_{3/2}$ to a final ground state.

The importance of coherent control techniques for such two-photon transitions to excited states is well established [23], with observed enhancements of up to a factor of 10 for suitable phase masks applied to the excitation pulses [24]. A resonant dense atomic medium itself acts as a phase mask for the ultrashort photonic wave packet, inducing strong distortions and leading to a shape known as zero-area pulse [25,26]. The observation of such zero-area pulse formation in an atomic medium for single photons from SPDC was actually the main motivation for the present work [6], since it demonstrates that these photons may be produced in a way to follow the dynamics of weak laser pulses coherently propagating in an atomic sample. A systematic investigation of absorption and storage of weak ultrashort laser pulses in atomic media becomes then an important step in the development of memory protocols for ultrashort single photons. Here we present our first results in this direction, quantifying and optimizing the absorption of a weak ultrashort laser pulse (signal) by a dense atomic ensemble. The pulse acts on the 795-nm $D1$ line of rubidium. Its absorption is enhanced by a stronger control pulse at 762 nm that transfers to level $5D_{3/2}$ any transient population induced by the weak pulse at level $5P_{1/2}$. This scheme, acting on different transitions, was introduced in 2002 to study the dynamics of transient populations induced by zero-area pulses acting on atomic ensembles [27]. Here we use this effect to enhance the transfer of energy from the weak light pulse to the material medium.

In the following, in Sec. II we introduce in more detail our scheme to enhance the absorption of ultra-broadband photons by a narrowband atomic medium. We include in this section a theory for the process still in the weak absorption regime, the relevant limit for the present stage of our experiments. In Sec. III, we describe the experimental setup for the absorption of the weak laser pulse and our characterization procedures. Section IV presents our results combining measurements and theory. Particularly, we focus on three optimization parameters: atomic density, power of control pulse, and delay between signal and control pulses. The pulses are shaped to be transform limited. We observe a maximum enhancement of absorption of 0.3%, but no strong saturation with atomic density or control power, which indicates a clear pathway to improve the system to attain high absorptions. We also did not explore here any spectral masks to improve absorption, being this the subject of a second stage of our experiment currently

under way. Finally, in Sec. V we offer our conclusions on the subject so far.

II. ENHANCED ABSORPTION IN THE ULTRA-BROADBAND REGIME

The resonant excitation of a two-level atom by a light pulse is commonly described in terms of the pulse area θ defined as

$$\theta = \int_{-\infty}^{+\infty} \frac{\mu \mathcal{E}(t)}{\hbar} dt,$$

with μ being the transition dipole moment, $\mathcal{E}(t)$ being the pulse's electric-field temporal envelope at the position of the atom, and \hbar being Planck's constant [28]. For an ultrashort pulse, we can neglect any decoherence process during excitation, and the population of the excited state would be given by $\rho_e = \sin^2(\theta/2)$. A π pulse, for example, would then lead to a total inversion of the atomic population.

We can estimate the area of an ultrashort single photon (temporal width $T \approx 100$ fs) acting on an atomic ensemble in common experimental situations. A single photon at 800 nm carries an energy of $hc/\lambda = 2.5 \times 10^{-19}$ J, with c being the velocity of light. If the photon propagates in a Gaussian mode focused to a transversal waist of $w = 50 \mu\text{m}$, its volume will be approximately $V = \pi w^2 \times cT \approx 2.4 \times 10^5 \mu\text{m}^3$. The energy density of a photon on this light mode will be then $u = (hc/\lambda)/V \approx 10^{-6}$ J/m³. The electric field associated with this energy density would be $|\mathcal{E}| \approx 500$ V/m. Approximating $\mu \approx ea_0$ for a typical dipole moment, with e being the electron's charge and a_0 being Bohr's radius, the single-photon pulse area would be around $\theta = \mu|\mathcal{E}|T/\hbar = 4 \times 10^{-6}$, leading to $\rho_e \approx 4 \times 10^{-12} = p_{11}$.

This number for the probability p_{11} to excite an atom by a single photon seems quite small at first sight. However, in hot atomic vapors it is straightforward to obtain atom numbers $N \gg 10^{12}$ in the photonic spatial mode assumed above. According to this simple analysis, we should be able to observe large absorptions of ultrashort single photons in common experimental conditions. The problem with this analysis so far is that it does not take into account the back action of such large atomic ensembles on the photonic mode, which leads, during propagation through the medium, to the formation of a zero-area pulse [25], a pulse with an area much smaller than the one in the entrance of the sample. Such zero-area pulses keep their energy throughout propagation, but become increasingly unable to leave any final excitation on the atoms. The zero-area pulse shape comes primarily from the dispersive part of the atom-light interaction, which becomes rapidly dominant over the absorptive part as the atomic density of the medium increases [29]. This process makes the direct single-photon absorption by the resonant sample of two-level atoms effectively unattainable, since the pulse area rapidly decreases as the number of atoms increases [6].

On the other hand, cascaded two-photon transitions to higher excited states induced by weak ultrashort pulses are commonly observed [30,31], with the connection to transient population excitation in the lower transition, in which the zero-area pulse is formed, clearly established in Ref. [27]. Such transient excitations are much larger than the final area

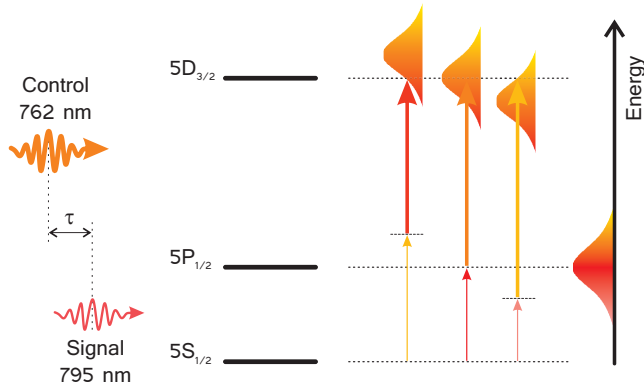


FIG. 1. Schematic of the two-photon combinations for cascaded excitations in rubidium atoms. The $5P$ state enables the occurrence of stepwise two-photon excitations, involving the $5S \rightarrow 5P$ (795 nm) and $5P \rightarrow 5D$ (762 nm) transitions. The pulses acting on each transition arrive in the sample with a controllable relative delay τ .

of the pulse. In order to keep the total energy of the pulse ($\propto |\mathcal{E}|^2$) roughly constant while decreasing the pulse area ($\propto \mathcal{E}$), the pulse's electric field develops a tail that periodically inverts its sign to cancel the excitation generated by its previous portions. In this way, the zero area is established through a series of relatively strong transient excitations of different signs. These previous observations suggest then an alternative approach for the absorption of a single photon by an atomic medium, in which a control pulse of similar bandwidth would excite the atom to a higher state at a transient peak of excitation in the lower transition, in order to maximize the transfer of energy to the atomic medium [27]. In frequency space, the feasibility of this approach comes from the fact that such two-photon transitions are intrinsically broadband. As illustrated in Fig. 1 for the cascade $5S \rightarrow 5P_{1/2} \rightarrow 5D$ transition in rubidium, if the central frequencies of the signal and control pulses are resonant, respectively, with each of the transitions on the cascade, then any other frequency on the weak-pulse spectrum will find another frequency on the control field to close the two-photon transition. In the following, we develop a detailed model of this process to compare later with our experimental data at the low excitation regime.

A. Theory

In order to understand the absorption process described above, we introduce a theory for the propagation of the signal pulse through the dense atomic medium in the condition illustrated in Fig. 1, i.e., of a two-photon cascaded excitation induced by a control pulse. Signal and control pulses propagate on the same z direction, and the control pulse has a delay τ with respect to the signal at the entrance of the medium. We approximate the atomic structure by a three-level system of the relevant hyperfine levels involved on the cascade transition, labeling the states $|0\rangle = |5S_{1/2}\rangle$, $|1\rangle = |5P_{1/2}\rangle$, and $|2\rangle = |5D_{3/2}\rangle$, respectively.

For very weak signal pulses, the population on level $|1\rangle$ is negligible, and the stronger control pulses pass through the ensemble without being affected by the atoms. At a position z , considering the pulses enter the ensemble

at $z = 0$, the electric field of the control pulse can be written then as $E_c(z, t) = E_c(0, t - \tau - z/c) = \mathcal{E}_c(t - \tau - z/c) \cos[\omega_c(t - \tau - z/c)]$, with $\mathcal{E}_c(t - \tau)$ being the slow pulse envelop at $z = 0$ and ω_c being the center frequency of the control field. For the signal pulse, on the other hand, we have to consider its full propagation throughout the dense ensemble. This is modeled by the respective Maxwell equation for the signal pulse electric field $E_s(z, t)$ [25]:

$$\frac{\partial \Omega_s}{\partial z} + \frac{1}{c} \frac{\partial \Omega_s}{\partial t} = i\alpha_0 \Gamma_{10} \int_{-\infty}^{\infty} d\Delta \sigma_{10}(\Delta) f_d(\Delta), \quad (1)$$

with $\Omega_s(z, t) = \mu_{01} \mathcal{E}_s(z, t)/\hbar$ being the respective instantaneous Rabi frequency, μ_{01} being the electric dipole moment for the transition $0 \rightarrow 1$, $\mathcal{E}_s(z, t)$ the signal-pulse slow envelop, α_0 being the medium absorption coefficient, Γ_{10} being the population decay rate from $|1\rangle$ to $|0\rangle$, $f_d(\Delta)$ being the Doppler distribution of atomic detunings Δ relative to the center frequency ω_s of the signal field, and σ_{01} being the slowly varying atomic coherence between levels $|1\rangle$ and $|0\rangle$. At the medium entrance, the electric field is $E_s(0, t) = \mathcal{E}_s(0, t) \cos(\omega_s t)$.

In order to calculate σ_{01} , we start with the Bloch equation for the coherence ρ_{01} :

$$\frac{\partial \rho_{01}}{\partial t} = \frac{i}{\hbar} \langle 0 | [\rho, H] | 1 \rangle - \frac{\Gamma_{10}}{2} \rho_{01}, \quad (2)$$

coming from the Hamiltonian

$$H = H_0 + V(\vec{r}, t), \quad (3)$$

with

$$H_0 = E_0 |0\rangle \langle 0| + E_1 |1\rangle \langle 1| + E_2 |2\rangle \langle 2|$$

being the free-atom Hamiltonian for the three levels with energies E_0 , E_1 , and E_2 , respectively, and

$$V(z, t) = -\mu_{01} E_s(z, t) |0\rangle \langle 1| - \mu_{12} E_c(z, t) |1\rangle \langle 2| + c.c.$$

being the interaction potential in the electric-dipole approximation, with μ_{12} being the electric dipole moment for the transition $1 \rightarrow 2$. It is straightforward to obtain an integral solution for σ_{01} in lowest order of the signal field amplitude, since strong approximations apply quite well in the limit of very weak signal fields, the relevant regime for single-photon storage. We may safely suppose the populations are unaffected by the excitation pulses, i.e., $\rho_{00} \approx 1$ and $\rho_{11} \approx \rho_{22} \approx 0$. As a result, we have

$$\sigma_{01}(z, t) \simeq \int_{-\infty}^t dt' e^{-(\Gamma_{10}/2 + i\Delta)(t-t')} \left[i \frac{\Omega_s(z, t')}{2} - \frac{\Omega_c^*(z, t')}{2} \int_{-\infty}^{t'} dt'' \frac{\Omega_c(z, t'')}{2} \sigma_{01}(z, t'') \right], \quad (4)$$

with $\Omega_c(z, t) = \mu_{12} \mathcal{E}_c(z, t)/\hbar$ being the instantaneous Rabi frequency for the control field. We extended the time origin to $-\infty$, since both pulses are zero in this limit. Note that we kept the factor $e^{-(\Gamma_{10}/2 + i\Delta)(t-t')}$ on the first integral over t' , but neglected the similar factors on other integrals involving its multiplication by the signal or control pulses, since these are much shorter than any time for which these factors would deviate significantly from one [32].

The lowest order solution of Eq. (4) in both Ω_s and Ω_c is then

$$\sigma_{01}(z, t) \simeq i \int_{-\infty}^t dt' e^{-(\Gamma_{10}/2 + i\Delta)(t-t')} \left[\frac{\Omega_s(z, t')}{2} - \frac{\Omega_c^*(z, t')}{2} \int_{-\infty}^{t'} dt'' \frac{\Omega_c(z, t'')}{2} \int_{-\infty}^{t''} dt''' \frac{\Omega_s(z, t''')}{2} \right]. \quad (5)$$

At this point, it is important to define two auxiliary function:

$$\theta_s(z, t) = \int_{-\infty}^t dt' \Omega_s(z, t'), \quad (6a)$$

$$\theta_c(z, t) = \int_{-\infty}^t dt' \Omega_c(z, t'), \quad (6b)$$

which represent the area of each pulse at position z of the ensemble, up to a time t . These are slowly varying functions compared to the respective pulses, being close to a step function for a short well-behaved pulse. Since they are slow, they can be approximated by constant values, inside the higher order integrals on the right hand side of Eq. (5), on the instant the control pulse reaches the position z . Equation (5) then becomes

$$\sigma_{01}(z, t) \simeq i \int_{-\infty}^t dt' e^{-(\Gamma_{10}/2 + i\Delta)(t-t')} \left[\frac{\Omega_s(z, t')}{2} - \frac{1}{8} \Omega_c^*(z, t') \theta_s(z, \tau + z/c) \frac{\Theta_c}{2} \right], \quad (7)$$

with $\Theta_c = \theta_c(0, t \rightarrow \infty)$ being the control pulse area at $z = 0$. Note that we assume a well-behaved control pulse on the beginning of the ensemble that remains unchanged during its propagation. The evaluation of this pulse area exactly on the instant of its action on the ensemble can be approximated, then, by half of its total area, as for a well-behaved step function exactly on the position of the step. The function $\theta_s(z, \tau + z/c)$, however, is much more delicate, since the signal pulse may be strongly distorted during its propagation up to z and is acted upon by the unperturbed control pulse traveling at essentially vacuum speed up to the same point. Thus, some degree of temporal walk-off may occur in the process.

This equation can finally be substituted on Eq. (1), resulting in

$$\frac{\partial \Omega_s}{\partial z} + \frac{1}{c} \frac{\partial \Omega_s}{\partial t} = -\alpha_0 \int_{-\infty}^t dt' G(t-t') \left[\Omega_s(z, t') - \Omega_c^*(z, t') \theta_s(z, \tau + z/c) \frac{\Theta_c}{8} \right], \quad (8)$$

with

$$G(t-t') = \frac{\Gamma_{10}}{2} \int_{-\infty}^{\infty} d\Delta f_d(\Delta) e^{-(\Gamma_{10}/2 + i\Delta)(t-t')}. \quad (9)$$

Taking the Fourier transform of both sides of Eq. (8), we finally obtain

$$\left[\frac{\partial}{\partial z} - \frac{i\omega}{c} + \alpha_0 A(\omega) \right] \tilde{\Omega}_s(z, \omega) = \alpha_0 A(\omega) \tilde{\Omega}_c^*(z, -\omega) \theta_s(z, \tau + z/c) \frac{\Theta_c}{8}, \quad (10)$$

with

$$A(\omega) = \frac{\Gamma_{10}}{2} \int_{-\infty}^{\infty} d\Delta \frac{f_d(\Delta)}{\Gamma_{10}/2 - i(\omega - \Delta)}, \quad (11)$$

and $\tilde{\Omega}_s$ and $\tilde{\Omega}_c$ being the Fourier transforms for the respective instantaneous Rabi frequencies, and ω being the frequency components defined in relation to the pulse's central frequency. From Eq. (10), one verifies that each signal-pulse frequency component ω is affected by the frequency component of the control pulse on the other side of its spectrum ($-\omega$), as depicted in Fig. 1. Besides that, the overall action of the control pulse depends on multiple aspects of the problem. The factor $\theta_s(z, \tau + z/c)$ represents the excitation of atoms by the signal pulse to level $|1\rangle$ up to the instant the control field acts on that position of the ensemble [27]. The transfer of excitation from $|1\rangle$ to $|2\rangle$ is governed by the total area Θ_c of the control pulse.

If there is no control field, $\Omega_c = 0$, the solution to Eq. (10) at high densities develops the well-known zero-area pulse shape [6,25,30]. In frequency space, it is given by

$$\tilde{\Omega}_s^{(0)}(z, \omega) = \tilde{\Omega}_s(0, \omega) e^{[\frac{i\omega}{c} - \alpha_0 A(\omega)]z}. \quad (12)$$

The total pulse energy would be then

$$U^{(0)}(z) = \epsilon \int_{-\infty}^{\infty} d\omega |\tilde{\Omega}_s^{(0)}(z, \omega)|^2 = \epsilon \int_{-\infty}^{\infty} d\omega |\tilde{\Omega}_s(0, \omega) e^{-\alpha_0 \text{Re}A(\omega)z}|^2, \quad (13)$$

with ϵ being a proportionality constant. Mathematically, the low absorption of the ultra-broadband photon, when propagating through a resonant atomic medium, comes from the fact that $\text{Re}A(\omega)$ is a very narrow function when compared to $\tilde{\Omega}_s(0, \omega)$, decaying with ω^2 from resonance [see Eq. (11)]. The absorption represented by $e^{-\alpha_0 \text{Re}A(\omega)z}$ thus affects only a small portion of the pulse energy. The strong, fast distortions of the zero-area pulse comes from the dispersive action of the medium, proportional to $\text{Im}A(\omega)$, which is a much broader function decaying only with ω away from resonance. On the other hand, the right side of Eq. (10) involves a multiplication of $A(\omega)$ by the complex function θ_s , which then maps the dispersive part of $A(\omega)$ into the medium's absorption coefficient, leading to an overall larger absorption.

In order to proceed with the treatment for the action of the control pulse, note first that Eq. (10) can be written as

$$\frac{\partial}{\partial z} f(z, \omega) = \alpha_0 A(\omega) e^{[-\frac{i\omega}{c} + \alpha_0 A(\omega)]z} \tilde{\Omega}_c^*(z, -\omega) \times \theta_s(z, \tau + z/c) \frac{\Theta_c}{8}, \quad (14)$$

with

$$f(z, \omega) = e^{[-\frac{i\omega}{c} + \alpha_0 A(\omega)]z} \tilde{\Omega}_s(z, \omega). \quad (15)$$

In terms of the control field spectrum in the beginning of the sample $\tilde{\Omega}_c(0, \omega)$, we have

$$\tilde{\Omega}_c^*(z, -\omega) = \tilde{\Omega}_c^*(0, -\omega)e^{i\omega(\tau+z/c)}. \quad (16)$$

On the other hand, the signal pulse area in Eq. (14) can be written as

$$\begin{aligned} \theta_s(z, \tau + z/c) &= \int_{-\infty}^{\tau+z/c} dt \Omega_s(z, t) \\ &= \frac{1}{\sqrt{2\pi}} \int_{-\infty}^{\tau} dt \int_{-\infty}^{\infty} d\omega' e^{-i\omega'z/c} \tilde{\Omega}_s(z, \omega') e^{-i\omega't} \\ &= \frac{1}{\sqrt{2\pi}} \int_{-\infty}^{\tau} dt \int_{-\infty}^{\infty} d\omega' e^{-\alpha_0 A(\omega')z} f(z, \omega') e^{-i\omega't}. \end{aligned} \quad (17)$$

Substituting Eqs. (16) and (17) into Eq. (14) and defining $\beta = \frac{\alpha_0 \Theta_c}{8}$, we have

$$\begin{aligned} \frac{\partial}{\partial z} f(z, \omega) &= \frac{\beta A(\omega)}{\sqrt{2\pi}} e^{i\omega\tau + \alpha_0 A(\omega)z} \tilde{\Omega}_c^*(0, -\omega) \\ &\quad \times \int_{-\infty}^{\tau} dt \int_{-\infty}^{\infty} d\omega' e^{-\alpha_0 A(\omega')z} f(z, \omega') e^{-i\omega't}. \end{aligned} \quad (18)$$

By integrating Eq. (18) from 0 to z on both sides, the differential equation turns into an integral equation, more suitable to a perturbative analysis:

$$\begin{aligned} f(z, \omega) &= f(0, \omega) + \int_0^z dz' \frac{\beta A(\omega)}{\sqrt{2\pi}} e^{i\omega\tau + \alpha_0 A(\omega)z'} \tilde{\Omega}_c^*(0, -\omega) \\ &\quad \times \int_{-\infty}^{\tau} dt \int_{-\infty}^{\infty} d\omega' e^{-\alpha_0 A(\omega')z'} f(z', \omega') e^{-i\omega't}. \end{aligned} \quad (19)$$

Lowest order solution in Θ_c

Expanding Eq. (19) to the lowest order in Θ_c , we obtain

$$\begin{aligned} f^{(1)}(z, \omega) &= f(0, \omega) + \int_0^z dz' \frac{\alpha_0 \Theta_c A(\omega)}{8\sqrt{2\pi}} e^{i\omega\tau + \alpha_0 A(\omega)z'} \\ &\quad \times \tilde{\Omega}_c^*(0, -\omega) \int_{-\infty}^{\tau} dt \int_{-\infty}^{\infty} d\omega' e^{-\alpha_0 A(\omega')z'} \tilde{\Omega}_s(0, \omega') e^{-i\omega't}. \end{aligned} \quad (20)$$

Equation (20) may be evaluated and gives directly the signal pulse at the end of the sample, $z = l$, with l being the sample length and $D = \alpha_0 l$ being the total optical depth of the sample. However, in order to compare with the experimental data in Sec. III, Eq. (20) must be modified to account for the fact that the control pulse is focused at the center of the sample and that its waist varies along z . Also, one must note that the signal in Eq. (20) depends on Ω_c squared. Effectively, the relevant interaction between signal and control pulses will occur only around the focus in a smaller region with length l_c given by twice the Rayleigh length of the control field spatial mode. In this region, the control pulse area can be approximated roughly as a constant with a value close to its maximum at the focus, as assumed by the theory. In Eq. (20), this modification is easily introduced by considered Θ_c constant but different from zero only in a region of $\pm l_c/2$ around $l/2$, the center

of the vapor cell. A second optical depth needs then to be introduced: $D_c = \alpha_0 l_c$, the optical depth of the interaction region.

With these considerations in mind, we can finally define the function

$$F(\omega, t) = \frac{1}{\sqrt{2\pi}} \int_{-\infty}^{\infty} d\omega' e^{-i\omega't} \tilde{\Omega}_s(0, \omega') \tilde{\Omega}_c^*(0, -\omega) T(\omega, \omega'), \quad (21)$$

with

$$\begin{aligned} T(\omega, \omega') &= \frac{A(\omega) e^{-D[A(\omega)+A(\omega')]/2}}{[A(\omega) - A(\omega')]} \\ &\quad \times \{e^{D_c[A(\omega)-A(\omega')]/2} - e^{-D_c[A(\omega)-A(\omega')]/2}\}, \end{aligned} \quad (22)$$

and write

$$\tilde{\Omega}_s^{(1)}(l, \omega) = \tilde{\Omega}_s^{(0)}(l, \omega) + \frac{\Theta_c}{8} e^{i\omega(\tau+l/c)} \int_{-\infty}^{\tau} dt F(\omega, t), \quad (23)$$

providing directly the modification of Eq. (12) by the control pulse in first order.

In the following, we will also approximate the general Voigt profile of Eq. (11), by the considerably simpler function

$$A(\omega) = \frac{1}{1 - i\omega T_2}, \quad (24)$$

which captures the essential physical aspects of the problem [6,33] by approximating the line shape to a Lorentzian profile with width given by the inverse of the inhomogeneous decay time T_2 of the atomic coherence. This form for $A(\omega)$ also allows us to write

$$\frac{A(\omega)}{[A(\omega) - A(\omega')]} = -\frac{(\omega' T_2 + i)}{(\omega - \omega') T_2}. \quad (25)$$

With this result, note that the integrand in Eq. (21) is proportional to $\tilde{\Omega}_s(0, \omega') \tilde{\Omega}_c^*(0, -\omega) / (\omega - \omega')$, which implies in a contribution for the atomic excitation in the form expected from Fig. 1, i.e., a two-photon resonance when a particular frequency of the signal pulse acts with the corresponding complementary frequency of the control pulse.

III. EXPERIMENT

Our experimental setup to implement the process depicted in Fig. 1 is shown in Fig. 2. Note that we assumed a stronger control pulse at 762 nm, on the $5P_{1/2} \rightarrow 5D$ transition of Rb, acting on the sample together with a weak signal pulse at 795 nm, on the $5S \rightarrow 5P_{1/2}$ transition. Both pulses should be ultrashort, in the fs regime. This is achieved first by tuning a mode-locked titanium-sapphire laser to 762 nm. In this condition, it delivers 650 mW of output power, with pulse widths of about 90 fs and repetition rate of 82 MHz. The pulse durations at all stages of our experiment were measured by an autocorrelation setup using a noncollinear second-order-harmonic generation geometry [34]. The laser output is then split into two beams by a half-wave plate (HWP) and a polarizing beam splitter (PBS), with 85% of its power moving forward to provide the control field and the remaining 15% being deflected to generate the signal field.

The weaker signal beam passes through a Faraday isolator (FI) before being coupled into a photonic crystal fiber (PCF),

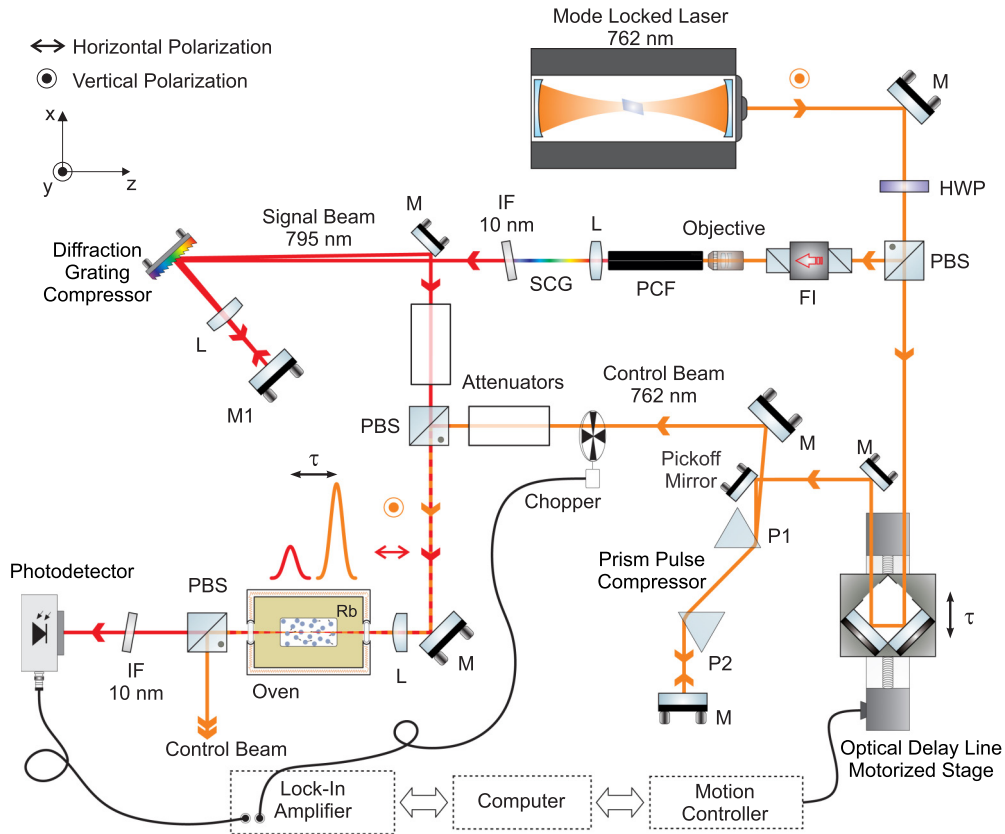


FIG. 2. Schematic view of the experimental setup. A Ti:Sapphire laser beam is split into signal and control beams. The first is coupled into a photonic crystal fiber (PCF) to generate a supercontinuum beam. Part of its spectrum is employed as the signal beam. The second beam is used as the control field. A linear translation stage in the control beam permits us to observe a time-resolved signal. The two-photon transition is realized with nearly transform limited pulses. SCG, supercontinuum beam; FI, faraday isolator; IF, interference filters; PBS, polarizing beam splitter; HWP, half-wave plate; attenuator, combination of HWP and PBS; M, mirrors; and L, lens.

FemtoWhite 800-NKT Photonics, using a Newport M-40 \times objective lens. After the PCF, we have a supercontinuum (SCG) beam with significant spectral power extending from 600 to 850 nm. The FI is fundamental in this setup, since it eliminates feedback to the laser oscillator. Furthermore, it increases the pulse chirp and optimizes supercontinuum generation in the PCF. The SCG beam is filtered by a tilted interference filter, centered at 800 nm and with a bandwidth of 10 nm, resulting in a transmitted beam around 795 nm [35] (see the Appendix). A pulse compressor, with a diffraction grating (1200 lines/mm) is used to obtain a nearly transform limited signal beam, with duration of 120 fs and bandwidth of 7.5 nm FWHM in the Rb cell region.

The control beam is directed to a computer controlled linear translation stage in order to scan the delay τ between control and signal pulses. The translation stage is adjusted to provide the delay τ at the entrance of the vapor cell. Dispersion occurs as the ultrashort control beam interacts with optical elements that directs it to the Rb cell. In order to obtain a transform-limited pulse in the cell, it is used a prism pair pulse compressor, as depicted in Fig. 2. The compressor introduces a negative dispersion that is compensated as the beam travels, in order to obtain a transform-limited control pulse in the Rb-cell region, with pulse width of 84 fs.

Before being recombined, the control and signal beams pass through different attenuators (a combination of HWP

and PBS) in order to obtain an absorption signal that can be investigated as function of the control and signal intensities, independently. Both beams are linearly polarized, with orthogonal polarizations with respect to each other. The beams are recombined in a PBS and focused at the center of a 5-cm Rb cell, each having a spot size of $\approx 125 \mu\text{m}$, and maximum time-averaged powers of 0.8 mW for the signal and 170 mW for the control field. The Rb cell is mounted inside an oven, and its temperature may be varied between 20 and 150 $^{\circ}\text{C}$, allowing us to control the atomic density.

After the Rb cell, a PBS reflects the control beam and transmits the signal beam. A tilted interference filter, centered at 800 nm and with bandwidth of 10 nm, is placed to block any remnant light from the control beam. The detection apparatus consists of a photodetector (2307 New Focus), and a lock-in amplifier, locked to the chopper reference frequency f_{ref} . The chopper is placed in the pathway of the control field. Thus, the lock-in amplifier outputs the difference in the signal beam transmission through the cell with and without control field. In terms of the theoretical quantities calculated in Sec. II A, the signal would be proportional to

$$\Delta U = U^{(0)}(I) - U^{(1)}(I), \quad (26)$$

with $U^{(1)}(I)$ calculated as $U^{(0)}(I)$, but with the field from Eq. (23). On the other hand, $U^{(0)}(I)$ is measured by placing the chopper on the signal beam and blocking the control beam.

From these two measurements, we obtain the variation of the absorption coefficient

$$\Delta\alpha = \frac{\Delta U}{U^{(0)}(l)}, \quad (27)$$

which is caused by the presence of the control pulse. This is the quantity which is compared to our theoretical predictions. More specifically, we are interested in its maximum value $\Delta\alpha_{\max}$ as a function of τ , for a particular set of parameters, such as atomic density and control power.

For an absorption signal of $135 \mu\text{V}$ in the lock-in amplifier, a typical value for our maximum absorption, we would have a noise floor around $2.3 \pm 0.8 \mu\text{V}$ coming from light at 795 nm . This was measured by blocking the chopped control beam. At the same conditions, blocking the signal beam, our noise floor for the control light at 762 nm was around $1.98 \pm 0.09 \mu\text{V}$. The electronic noise floor was around $0.3 \pm 0.2 \mu\text{V}$.

IV. RESULTS AND DISCUSSION

Figure 3 presents our measurements for $\Delta\alpha$ as a function of τ for various atomic densities η of the medium (black solid lines). The oven temperature changed from 85 up to 145°C , with the respective change of η from 1.7×10^{12} to $6.5 \times 10^{13} \text{ cm}^{-3}$. For the control and signal average powers of Sec. III, the experimental estimated pulse areas are $\Theta_c^{\text{exp}} \approx 0.36 \text{ rad}$ and $\Theta_s^{\text{exp}} \approx 0.06 \text{ rad}$, respectively. When the delay τ is scanned further, the absorption enhancement presents oscillations akin to the ones observed for the zero area pulses, as expected for this low-perturbation regime.

We consider Gaussian shapes for the temporal profile of both control and signal pulses, with durations $T_c = 84 \text{ fs}$ and $T_s = 190 \text{ fs}$, respectively. To properly fit the data, T_s must be increased in relation to the respective experimental value. We understand this is a consequence of our theory supposing the control pulse to be much shorter than the signal pulse, $T_c \ll T_s$, which is not the case in the experiment. The larger value of T_s therefore emulates the convolution between the two pulse durations. The fitting to the theoretical parameters was done for the curve with highest D . The others were generated by tuning D and T_2 according to the experimental values for atomic density and inhomogeneous decay time corresponding to each temperature.

The comparison to our theoretical model is provided by the respective dashed red curves on Fig. 3. For these, we changed the optical depth from $D = 19$ up to 720 . For this interval, the inhomogeneous broadening varies with the temperature, being given by the inverse of the full width of the expected Doppler broadening for the $|5S\rangle \rightarrow |5P_{1/2}\rangle$ transition, with T_2 going from 289 ps (for $D = 19$) down to 267 ps (for $D = 720$). The control and signal pulse areas in the beginning of the sample were assumed $\Theta_c = 0.20$ and $\Theta_s = 0.001$, respectively. As expected, the normalized $\Delta\alpha$ does not depend on Θ_s . The theoretical values for D and Θ_c are on the order of the expected experimental parameters, but an exact correspondence between them is not expected due to the simplicity of our three-level model. The actual atomic transitions present a large number of hyperfine and Zeeman sublevels. Also, the region around the focus which contribute to the signal was considered through the parameter $D_c = D/4$. If one assumes

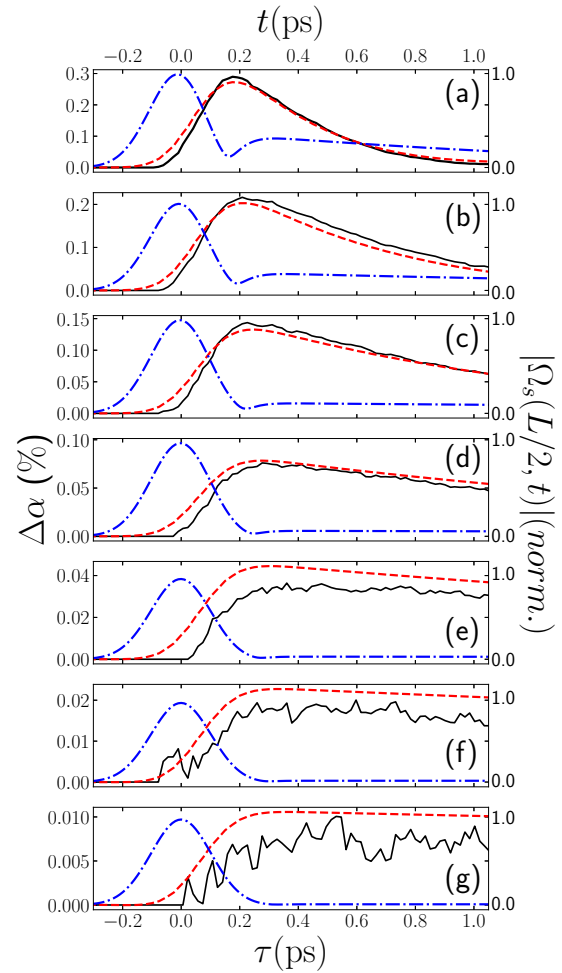


FIG. 3. Experimental (black solid lines) and theoretical (red dashed lines) enhanced absorption coefficient (left axis) as a function of the delay (bottom axis) between control and signal pulses for various atomic densities η . Corresponding modulus for the instantaneous Rabi frequency Ω_s (right axis, blue dash-dotted lines) of the signal pulse in the middle of the cell, as a function of time (top axis). The right axis in each panel was normalized so that Ω_s is plotted on the same scale as the corresponding $\Delta\alpha$. From top to bottom, we have (a) $\eta = 6.5 \times 10^{13} \text{ cm}^{-3}$ and $D = 720$, (b) $3.9 \times 10^{13} \text{ cm}^{-3}$ and 430 , (c) $2.2 \times 10^{13} \text{ cm}^{-3}$ and 240 , (d) $1.2 \times 10^{13} \text{ cm}^{-3}$ and 130 , (e) $0.7 \times 10^{13} \text{ cm}^{-3}$ and 73 , (f) $0.34 \times 10^{13} \text{ cm}^{-3}$ and 38 , (g) $0.17 \times 10^{13} \text{ cm}^{-3}$ and 19 . The other parameters are specified in the text.

longer regions, the theoretical predictions in Fig. 3 would present a slower decrease after the first maximum, since the signal would mix contributions from other parts of the ensemble with increasing differences in the oscillatory pattern.

We obtain a reasonable fit of the experimental data to our simplified model as we change the atomic density by a factor of 40. Particularly important for the purpose of our work is to predict the delay and height of the maximum enhancement of the absorption, and we see that the model captures properly this aspect of our experimental curves as the parameters are changed. In order to gain insight into these results, we also plot in Fig. 3, superposed to the results for $\Delta\alpha$, the normalized modulus of the unperturbed instantaneous Rabi

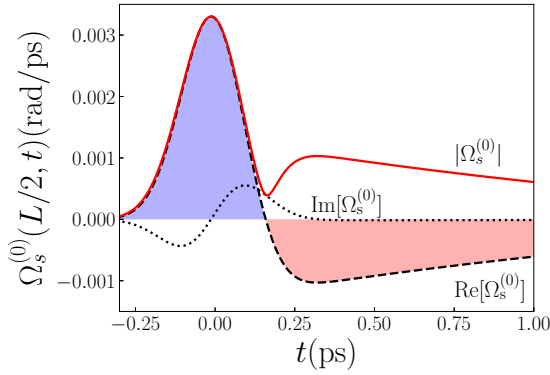


FIG. 4. Instantaneous Rabi frequency of the signal field as a function of time. The dashed and dotted black lines provide its real and imaginary parts, respectively. Its modulus is given by the solid red line. The area below the dashed line is blue for positive values and red for negative values.

frequency of the signal field, as a function of time, evaluated at the center of the sample, $|\Omega_s^{(0)}(L/2, t)|$, which is the region contributing most to the shape of the measured curve. For this superposition, we equate the time origin (top scale) with the delay origin (bottom scale), and normalized $|\Omega_s^{(0)}|$ (right scale) to fit on the same frame as $\Delta\alpha$ (left scale). $\Omega_s^{(0)}(z, t)$ was obtained from the inverse Fourier transform of Eq. (12) and was chosen for comparison because it is a well-known result and our theory on the regime of very small perturbation provides pulses with basically the same shape. We define $\Delta\alpha_M$ and τ_M , respectively, as the maximum enhancement and the pulse delay at which it occurs. Note that in all frames the delay τ_M happens where the maximum of the control pulse coincide with the minimum of $|\Omega_s^{(0)}|$.

This result, on the other hand, is better understood by examining Fig. 4, which shows the modulus of $\Omega_s^{(0)}(L/2, t)$ together with the real and imaginary parts of the same quantity for $D = 720$, corresponding to the parameters of Fig. 3(a). The minimum in $|\Omega_s^{(0)}(L/2, t)|$ (red solid line) occurs when $\text{Re}[\Omega_s^{(0)}(L/2, t)]$ changes sign. This is a typical situation for zero area pulses: The first part of the pulse transfers population to the excited state transiently, which is then removed by a second part of the pulse of inverted sign. This process is repeated over time throughout the whole pulse profile until no excitation is left on the medium. In our system, there is an imaginary portion of $\Omega_s^{(0)}(L/2, t)$ coming from a small experimental detuning of the signal field with respect to resonance, which prevents maximum transfer of population for a fixed initial pulse area. This process of transient excitation by zero area pulses was first discussed in Ref. [27], which largely inspired the present work, and it is a temporal analog to the process described in Fig. 1 in frequency space. In Fig. 4, the maximum transient area Θ_s^{tr} for that particular physical situation is indicated by the region in blue for positive values of $\text{Re}[\Omega_s^{(0)}(L/2, t)]$, resulting in $\Theta_s^{tr} \approx 7.3 \times 10^{-4}$ rad. The final area Θ_s^f beyond 600 ps is below 10^{-5} rad. As expected from a zero area pulse leaving no significant population on the excited state, $\Theta_s^f \ll \Theta_s$. However, the crucial point for the objectives of the present work is that we have $\Theta_s^{tr} \approx \Theta_s$, with

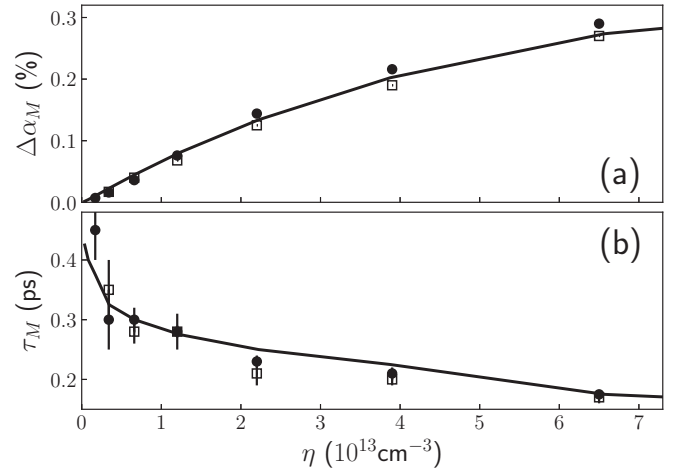


FIG. 5. Maximum enhancement of absorption $\Delta\alpha_M$ (a) and the delay τ_M (b) for which it happens as a function of the atomic density η . Solid circles and open squares are the experimental results (for different days) and the solid lines are the prediction from the theory. Parameters were the same as for Fig. 3.

a decrease in Θ_s^{tr} of only 27% with respect to the pulse area at the entrance of the medium.

The maximum enhancement $\Delta\alpha_M$ and its respective delay τ_M as a function of η are plotted on Fig. 5, together with the expected variation from the theory. For the purpose of photon storage, these two quantities are the central results of our experimental approach. The solid circles are the experimental values for these quantities obtained directly from the panels of Fig. 3 and the solid lines provide the theoretical results for the same parameters of Fig. 3. The error bars are quite small for $\Delta\alpha_M$. To evaluate systematic variations on the determination of the experimental conditions, we plot as open squares the results of a run of the same experiment on a different day under the same conditions. Note from Fig. 5(b) that a relatively strong walk-off between the two pulses should be observed for the largest atomic densities, with τ_M changing by about 200 fs from the beginning to the end of the sample. This is not critical for our present low-excitation regime, but may be an important issue once higher excitation probabilities are achieved and the system requires a fine optimization.

The same quantities as a function of the control-field average power P_c are plotted in Fig. 6. For the whole curve, η was kept at its maximum, 6.5×10^{13} atoms/cm³. The point of highest P_c in Fig. 6 is then taken at the same experimental conditions as the point of highest η in Fig. 5. The solid circles show the results of an experimental run turning P_c down, while the open square and diamond are different measurements at maximum P_c and η . We observe then an increase of $\Delta\alpha_M$ with P_c , while τ_M is kept almost constant. The theory follows qualitatively this overall behavior, but with worst comparison than for the variation with η . This could be expected from the various approximations in the theory related to the control power. First, in our final expression we considered only the lowest order solution on the control power from Eq. (19). Second, we neglected any intensity variation as the control field focus in the middle of the vapor cell, approximating the

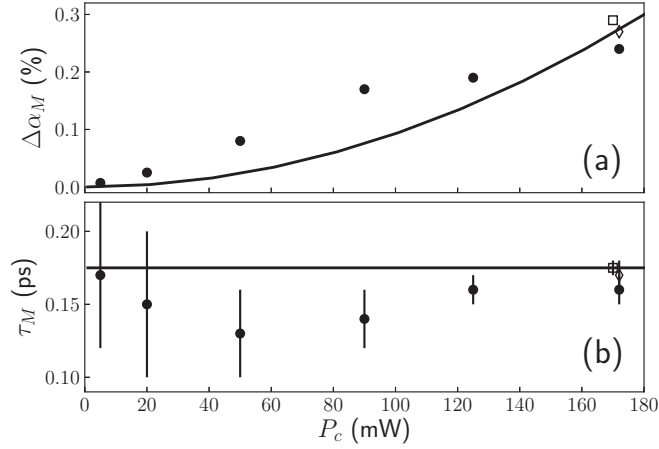


FIG. 6. Maximum enhancement of absorption $\Delta\alpha_M$ (a) and the delay τ_M (b) for which it happens as a function of the control power P_c . Solid circles are the experimental results and the solid lines the prediction from the theory. The open square and diamond are experimental points obtained at maximum P_c on different days. In the theory, the control electric field amplitude was scaled proportional to $\sqrt{P_c/P_c^{\max}}$, with P_c^{\max} being the maximum power. Other parameters were the same as for the maximum density in Fig. 3.

result for a constant intensity in a region of $l_c = l/4$ around its focus.

Finally, Fig. 7 plots the variation of both $\Delta\alpha_M$ and τ_M as a function of the signal-field power. There is no theoretical prediction for this variation. In Sec. II A, we employ a linear theory for the problem that results in no dependence with the initial signal power, as long as it is sufficiently small. Figure 7 was obtained for the maximum η and P_c of Figs. 5 and 6, and we observe that all measurements on Fig. 7 are consistent with the maximum values of these previous figures. This is crucial, since we aim at using the present investigation as a guide for future experiments with single photons, at much lower powers.

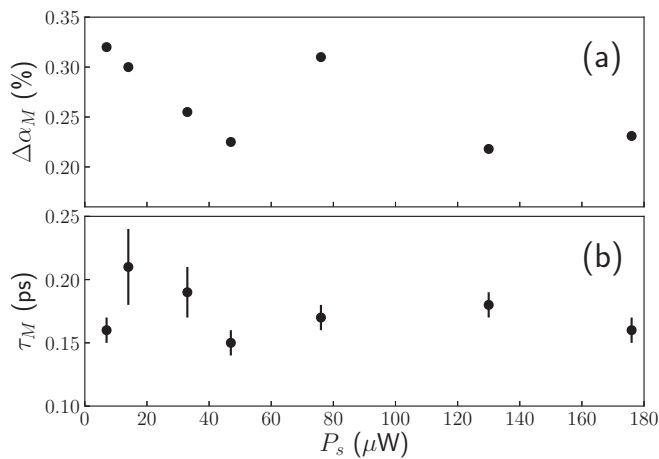


FIG. 7. Maximum absorption enhancement $\Delta\alpha_M$ (a) and the delay τ_M (b) for which it happens as a function of the signal power P_s . Other parameters are the same as for panel (a) of Fig. 3.

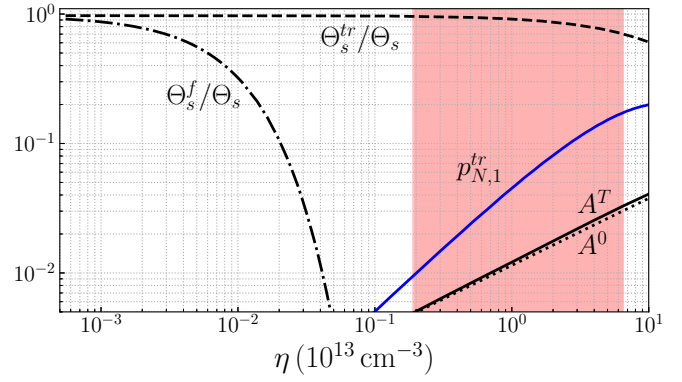


FIG. 8. Maximum transient signal pulse area Θ_s^{tr} (dashed black line) and final signal pulse area Θ_s^f (dash-dotted black line) as a function of the atomic density, normalized by the initial pulse area Θ_s . The colored area indicates the experimental range of our present investigation. A^0 is the expected absorption of a zero-area pulse (dotted black line) and A^T is the total absorption resulting from the action of the control pulse (solid black line). The blue line plots our estimation for the maximum transient probability of absorption for the total volume of the Gaussian beams inside the vapor cell. All other theoretical parameters were the same as for Fig. 3.

A. Pathway to high absorption

Up to now, we have developed the basic theory and experimental tools to enhance and characterize small absorptions of a weak ultrashort pulse by an atomic vapor. The enhancements observed so far were quite modest. However, these developments allow us to devise concrete strategies to proceed from here to the desired high absorption of a weak ultrashort pulse. The starting point is the discussion around Fig. 4 highlighting the role of the transient area Θ_s^{tr} of a zero area pulse to transfer a significant population in the beginning of its action in any particular portion of the atomic ensemble. Since the system is in the linear regime with respect to the signal pulse, when we normalize Θ_s^{tr} by the initial pulse area Θ_s , we have a function that describes the system's behavior down to the single-photon regime [6]. The same is valid for the normalization of the final area Θ_s^f by Θ_s . These two normalized quantities as a function of the atomic density are plotted in Fig. 8, with the dashed black line for Θ_s^{tr}/Θ_s and the dash-dotted black line for Θ_s^f/Θ_s . The dependence with η is obtained from the dependence with the optical depth D , as parametrized from Fig. 3. The atomic density variation of Fig. 8 corresponds to a temperature variation on the vapor cell from 22° up to 155°C , with the colored area indicating the atomic density span of the present investigation. Figure 8 quantifies then our previous observation that Θ_s^{tr} decreases much slower with η than Θ_s^f . It shows the fast decrease of the final pulse area in this low excitation regime, with a robust preservation of the initial area in the excitation transient.

Starting from the estimation, introduced in Sec. II, for the probability $p_{1,1}$ to excite a single atom by a single photon, we can estimate from Fig. 8 the maximum probability $p_{N,1}^{tr} = N f_{tr} p_{1,1}$ to excite one of N atoms by a single photon transiently, where $f_{tr} = (\Theta_s^{tr}/\Theta_s)^2$ and $N = \eta V_L$ is the number of atoms in the vapor-cell volume V_L interacting with the

optical beams. We estimate $V_L \approx 14 \times 10^{-3} \text{ cm}^3$. The curve for $p_{N,1}^r$ as a function of η is given by the solid blue line in Fig. 8. It predicts a maximum probability of about 17% for the maximum density of the present work. In order to compare with our present situation, it is crucial to estimate, using the theory for zero-area pulses, the total attenuation A^0 of the signal pulse predicted for our experimental conditions without the action of the control pulse. This quantity is plotted as a dotted black curve in Fig. 8. Θ_s^f may be extremely small, resulting in a pulse that does not leave any excitation in the atomic ensemble. However, energy is lost in the evolution from Θ_s to Θ_s^f due to the strong absorption of the pulse spectral components around the atomic line. This absorption slowly increases with η as the absorbed region of the spectrum increases. A^0 is small, around 2.9% for our maximum density, but for our present small excitation regime it is quite significant. The curve for the total absorption A^T enhanced by the control pulse in our present investigation is plotted as the solid black curve in Fig. 8, where we observe the slight increase by $\Delta\alpha \approx 0.3\%$ for our maximum density, already shown in Figs. 3 to 7. Note that $\Delta\alpha$ is the most directly accessible experimental quantity to characterize the absorption of the signal beam induced by the control field, but in the low excitation regime it is really just a small enhancement over the regular absorption present even for zero area pulses. On the other hand, $\Delta\alpha$ may be considered a total absorption if a high absorption regime is achieved and A^0 becomes negligible.

The maximum transient absorption given by $p_{N,1}^r$, considering the volume V_L of the present experiment, is still not very large when compared to A^0 , just a factor of 6. However, it reveals the most significant improvements to be pursued for the system. First, it becomes clear that there is no large gain in increasing η . The slight saturation appearing in the experimental data of Fig. 5 is probably a direct consequence of the decrease in Θ_s^r for our highest atomic densities, which ends up canceling the gains in atomic number for higher densities. The difference between $p_{N,1}^r$ and A^T , on the other hand, indicates that there are large gains to be expected in increasing the area of the control pulse. There are two main approaches that we envision to increase Θ_c . The first one is to move to a light source with higher pulse energies, either by introducing an amplifier to the present system or changing to a new laser. The second one is to devise a scheme of optical pumping to transitions with higher dipole moments, which may imply in changing the presently used transitions in rubidium or even the atomic species to better adapt to our light source. We expect the control power to enhance the absorption linearly, while the dipole moment should enhance it quadratically. Of course, exact numerical estimations have limited validity once the absorption increases more significantly, since the present low-excitation investigation serves only as an indication on how to improve the system. Once higher absorptions are achieved, the excitation dynamics should change considerably and we might witness even the suppression of the formation of the zero-area pulse.

At this point, it is essential to remember also that our approach employs so far the simplest possible pulse shapes: transform-limited Gaussian pulses. Our goal in using such simple pulse shape was to develop physical intuition on the

problem by keeping a close comparison between theory and experiment. This strategy has been successful up to this point, but limited us in terms of parameters to optimize the system. It is well known, for example, that transform-limited pulses are not the best choice to excite sequential two-photon transitions, with enhancements by a factor of 10 being observed for pulses deviating from this condition [24]. We are presently experimentally investigating the effects of such spectral masks in our system.

V. CONCLUSION

In the present work, we provided a detailed analysis of a process to enhance the absorption of a weak ultrashort pulse by a narrowband atomic medium. This proposal elaborates on ideas introduced in 2016, when a single-photon zero-area pulse was first observed and characterized [6]. This observation pointed to the possibility of employing well-known techniques for coherent control of atomic transitions by ultrashort pulses to the problem of devising a long-lived memory to a flying ultrashort single photon, such as the ones emitted in the process of parametric-down conversion. Particularly, our goal was to use the transient excitation of atoms by a zero-area pulse [27] to drain energy from the weak pulse, by means of a stronger ultrashort control pulse driving the transient excitation to a different atomic level not interacting with the weak pulse. We derived a propagation theory for this process, describing how the control pulse would affect, to lowest order, the final absorption of the weak pulse. We then compared this theory to experimental results and were able to corroborate the success of the original idea: to enhance absorption by the transient transfer of energy out of the transition interacting with the weak pulse. However, the maximum

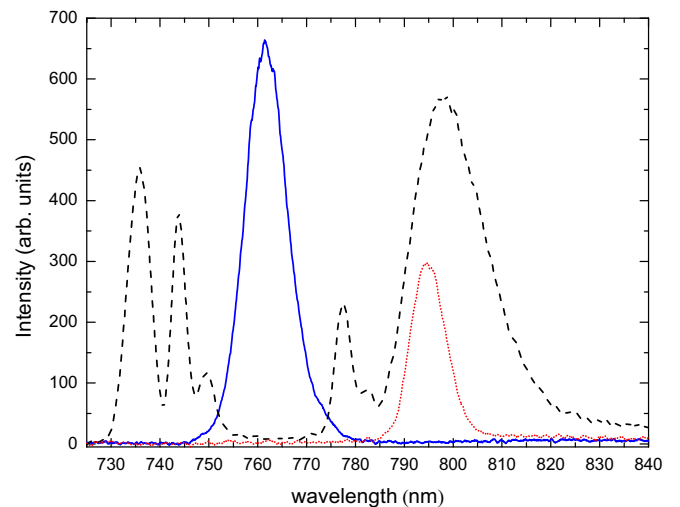


FIG. 9. Solid blue line is the spectrum for the laser at 762 nm. Dashed black line plots the supercontinuum generation (SCG) spectrum optimized for its spectral density around 800 nm. Dotted red line plots the spectrum of the SCG light after passing through the interference filter, which gives then our signal beam. Black and red lines are plotted to scale. The blue line is obtained from a small portion of the 762-nm light.

observed enhancement so far was quite modest, an increase of 0.3% on a pulse that should be already absorbed by 2.9% without the control pulse. Despite this fact, the complete set of observations and particularly the corroboration of our physical picture of the problem, by comparison with the theory, allowed us to devise different strategies to further advance the problem. We are now confident that our original goal is feasible. It should be possible to directly absorb, with high probability, an ultra-broadband single photon by a long-lived atomic memory.

ACKNOWLEDGMENTS

The authors acknowledges fruitful discussions with M. Bellini in the development on the present proposal. This work was supported by the Brazilian funding agencies CNPq (program INCT-IQ, No. 465469/2014-0), CAPES (program PROEX 534/2018, No. 23038.003382/2018-39), and FACEPE (program PRONEM 08/2014, No. APQ-1178-1.05/14).

APPENDIX: SPECTRA FOR SIGNAL-BEAM GENERATION

Figure 9 presents the relevant spectra of the fields involved in the generation of the signal beam at 795 nm. The solid blue line is the input spectrum from the laser, centered in 762 nm. The SCG spectrum for the light coming out of the PCF is given by the dashed black line. It typically spans from 600 up to 850 nm. However, its particular distribution in this region can be shaped by the alignment, power, and polarization of the input beam. We used 60 mW of 762-nm light at the entrance of the PCF. In Fig. 9, we show a typical SCG spectrum used in our experiment, which was then optimized to enhance its components around 800 nm. This SCG spectrum passes finally through the tilted interference filter, whose tilt angle is adjusted so that its center frequency is at 795 nm. For the SCG spectrum of Fig. 9, the corresponding signal-beam spectrum after the interference filter is given by the dotted red line. These two spectra are plotted with the same vertical scale in Fig. 9. The reduction in amplitude of the filtered spectrum comes from losses in the interference filter.

-
- [1] L. Mandel and E. Wolf, *Optical Coherence and Quantum Optics* (Cambridge University Press, Cambridge, UK, 1995).
 - [2] C. Couteau, Spontaneous parametric down-conversion, *Contemp. Phys.* **59**, 291 (2018).
 - [3] *The Physics of Quantum Information*, edited by D. Bouwmeester, A. Ekert, and A. Zeilinger (Springer-Verlag, Berlin, 2001).
 - [4] A. I. Lvovsky, B. C. Sanders, and W. Tittel, Optical quantum memory, *Nat. Photon.* **3**, 706 (2009).
 - [5] K. Heshami, D. G. England, P. C. Humphreys, P. J. Bustard, V. M. Acosta, J. Nunn, and B. J. Sussman, Quantum memories: Emerging applications and recent advances, *J. Mod. Opt.* **63**, 2005 (2016).
 - [6] L. S. Costanzo, A. S. Coelho, D. Pellegrino, M. S. Mendes, L. Acioli, K. N. Casemiro, D. Felinto, A. Zavatta, and M. Bellini, Zero-Area Single-Photon Pulses, *Phys. Rev. Lett.* **116**, 023602 (2016).
 - [7] M. D. Eisaman, A. André, F. Massou, M. Fleischhauer, A. S. Zibrov, and M. D. Lukin, Electromagnetically induced transparency with tunable single-photon pulses, *Nature (London)* **438**, 837 (2005).
 - [8] T. Chanelière, D. N. Matsukevich, S. D. Jenkins, S.-Y. Lan, T. A. B. Kennedy, and A. Kuzmich, Storage and retrieval of single photons transmitted between remote quantum memories, *Nature (London)* **438**, 833 (2005).
 - [9] E. Saglamyurek, T. Hrushevskiy, A. Rastogi, K. Heshami, and L. J. LeBlanc, Coherent storage and manipulation of broadband photons via dynamically controlled Autler-Townes splitting, *Nat. Photon.* **12**, 774 (2018).
 - [10] M. R. Sprague, P. S. Michelberger, T. F. M. Champion, D. G. England, J. Nunn, X.-M. Jin, W. S. Kolthammer, A. Abdolvand, P. St. J. Russell, and I. A. Walmsley, Broadband single-photon-level memory in a hollow-core photonic crystal fibre, *Nat. Photon.* **8**, 287 (2014).
 - [11] P. S. Michelberger, T. F. M. Champion, M. R. Sprague, K. T. Kaczmarek, M. Barbieri, X. M. Jin, D. G. England, W. S. Kolthammer, D. J. Saunders, J. Nunn, and I. A. Walmsley, Interfacing GHz-bandwidth heralded single photons with a warm vapour Raman memory, *New J. Phys.* **17**, 043006 (2015).
 - [12] X.-H. Bao, Y. Qian, J. Yang, H. Zhang, Z.-B. Chen, T. Yang, and J.-W. Pan, Generation of Narrow-Band Polarization-Entangled Photon Pairs for Atomic Quantum Memories, *Phys. Rev. Lett.* **101**, 190501 (2008).
 - [13] M. Scholz, L. Koch, and O. Benson, Statistics of Narrow-Band Single Photons for Quantum Memories Generated by Ultrabright Cavity-Enhanced Parametric Down-Conversion, *Phys. Rev. Lett.* **102**, 063603 (2009).
 - [14] F. Wolgramm, Y. A. de Icaza Astiz, F. A. Beduini, A. Cerè, and M. W. Mitchell, Atom-Resonant Heralded Single Photons by Interaction-Free Measurement, *Phys. Rev. Lett.* **106**, 053602 (2011).
 - [15] H. Zhang, X.-M. Jin, J. Yang, H.-N. Dai, S.-J. Yang, T.-M. Zhao, and J. Rui, Y. He, X. Jiang, F. Yang, G.-S. Pan, Z.-S. Yuan, Y. Deng, Z.-B. Chen, X.-H. Bao, S. Chen, B. Zhao, and J.-W. Pan, Preparation and storage of frequency-uncorrelated entangled photons from cavity-enhanced spontaneous parametric downconversion, *Nat. Photon.* **5**, 628 (2011).
 - [16] C. Clausen, I. Usmani, F. Bussières, N. Sangouard, M. Afzelius, H. de Riedmatten, and N. Gisin, Quantum storage of photonic entanglement in a crystal, *Nature (London)* **469**, 508 (2011).
 - [17] E. Saglamyurek, N. Sinclair, J. Jin, J. A. Slater, D. Oblak, F. Bussières, M. George, R. Ricken, W. Sohler, and W. Tittel, Broadband waveguide quantum memory for entangled photons, *Nature (London)* **469**, 512 (2011).
 - [18] M. Shapiro and P. Brumer, *Quantum Control of Molecular Processes* (Wiley-VCH, Weinheim, 2012).
 - [19] P. J. Bustard, R. Lausten, D. G. England, and B. J. Sussman, Toward Quantum Processing in Molecules: A THz-Bandwidth Coherent Memory for Light, *Phys. Rev. Lett.* **111**, 083901 (2013).

- [20] P. J. Bustard, J. Erskine, D. G. England, J. Nunn, P. Hockett, R. Lausten, M. Spanner, and B. J. Sussman, Nonclassical correlations between terahertz-bandwidth photons mediated by rotational quanta in hydrogen molecules, *Opt. Lett.* **40**, 922 (2015).
- [21] D. G. England, K. A. G. Fisher, J.-P. W. MacLean, P. J. Bustard, R. Lausten, K. J. Resch, and B. J. Sussman, Storage and Retrieval of THz-Bandwidth Single Photons using a Room-Temperature Diamond Quantum Memory, *Phys. Rev. Lett.* **114**, 053602 (2015).
- [22] B. Fang, S. Dong, S. Meiselman, O. Cohen, and V. O. Lorenz, Storage of ultra-broadband pulses in hot atomic barium vapor, in *Proceedings of the Conference on Lasers and Electro-Optics*, OSA Technical Digest (Optical Society of America, Washington, DC, 2017), paper FM2E.3, https://doi.org/10.1364/CLEO_QELS.2017.FM2E.3.
- [23] D. Meshulach and Y. Silberberg, Coherent quantum control of two-photon transitions by a femtosecond laser pulse, *Nature (London)* **396**, 239 (1998).
- [24] N. Dudovich, B. Dayan, S. M. Gallagher Faeder, and Y. Silberberg, Transform-Limited Pulses are Not Optimal for Resonant Multiphoton Transitions, *Phys. Rev. Lett.* **86**, 47 (2001).
- [25] M. D. Crisp, Propagation of small-area pulses of coherent light through a resonant medium, *Phys. Rev. A* **1**, 1604 (1970).
- [26] J. E. Rothenberg, D. Grischkowsky, and A. C. Balant, Observation of the Formation of the 0π Pulse, *Phys. Rev. Lett.* **53**, 552 (1984).
- [27] N. Dudovich, D. Oron, and Y. Silberberg, Coherent Transient Enhancement of Optically Induced Resonant Transitions, *Phys. Rev. Lett.* **88**, 123004 (2002).
- [28] L. Allen and J. H. Eberly, *Optical Resonance and Two-Level Atoms* (Dover, New York, 1987).
- [29] M. A. Bouchène, A. Débarre, J.-C. Keller, J.-L. Le Gouët, and P. Tchénio, Observation of 0π -pulse formation with incoherent light, *J. Opt. Soc. Am. B* **9**, 281 (1992).
- [30] D. Felinto, L. H. Acioli, and S. S. Vianna, Temporal coherent control of a sequential transition in rubidium atoms, *Opt. Lett.* **25**, 917 (2000).
- [31] D. Felinto, L. H. Acioli, and S. S. Vianna, Accumulative effects in the coherence of three-level atoms excited by femtosecond-laser frequency combs, *Phys. Rev. A* **70**, 043403 (2004).
- [32] D. Felinto and C. E. E. López, Theory for direct frequency-comb spectroscopy, *Phys. Rev. A* **80**, 013419 (2009).
- [33] U. Kallmann, S. Brattke, and W. Hartmann, Propagation of resonant 0π pulses in rubidium, *Phys. Rev. A* **59**, 814 (1999).
- [34] See, for example, Sec. 3.4 of *Ultrafast Optics* by A. M. Weiner (John Wiley & Sons, Hoboken, NJ, 2009).
- [35] The actual wavelength used was 794.3 nm, which was taken into account in all theoretical calculations.

Correction: The label τ was rendered incorrectly during the production process in two locations in Fig. 2 and has been fixed.